JOURNAL OF SOLID STATE CHEMISTRY **141,** 514–521 (1998)
ARTICLE NO. SC988007

Perovskite-Type $Ca_{1-x}Sr_xNbO_3$ ($0 \leq x \leq 1$) Phases: A Synthesis, Structure, and Electron Microscopy Study

S. Ya. Istomin,* G. Svensson,†,[1] O. G. D'yachenko,* W. Holm,‡ and E. V. Antipov*

* *Chemical Department, Moscow State University, 119899 Moscow, Russia;* † *Arrhenius Laboratory, Department of Structural Chemistry, Stockholm University, S-106 91 Stockholm, Sweden; and* ‡ *Department of Solid State Physics, The Royal Institute of Technology, S-100 44 Stockholm, Sweden*

Received April 27, 1998; in revised form August 13, 1998; accepted August 14, 1998

Reduced niobates $Ca_{1-x}Sr_xNbO_3$ ($0 \leq x \leq 1$) with perovskite-type structures have been synthesized at 1500°C in niobium ampoules sealed under argon gas. The prepared compounds were characterized by X-ray powder diffraction, electron diffraction, high-resolution electron microscopy, and energy-dispersive X-ray analysis. The structure of $CaNbO_3$ ($GdFeO_3$ type) was refined using X-ray powder diffraction data. Electron diffraction studies showed that complex superstructures of the perovskite-type structure occur for $x > 0$ in $Ca_{1-x}Sr_xNbO_3$: (i) for $x = 0.2$ and 0.3 reflections corresponding to a supercell with $a \approx 2 \times \sqrt{2} \times a_{per}$, $b \approx 4 \times a_{per}$, and $c \approx 2 \times \sqrt{2} \times a_{per}$ (per = ideal perovskite) were observed, (ii) for $x = 0.5$, 0.6, and 0.7 a cubic supercell was found with $a = 4 \times a_{per}$, whereas (iii) for $x = 0.8$ and 0.9 the supercell is probably orthorhombic with $a \approx c \approx \sqrt{2} \times a_{per}$ and $b \approx 2 \times a_{per}$. For $x = 1.0$ a new orthorhombic modification of $SrNbO_3$ with $a \approx c \approx \sqrt{2} \times a_{per}$ and $b \approx 2 \times a_{per}$ was found. Resistivity measurements showed $CaNbO_3$ to have a nonmetallic type of conductivity, whereas the Sr-containing samples were metallic. © 1998 Academic Press

INTRODUCTION

Complex transition metal oxides with perovskite-like structures are known to exhibit widely differing physical properties, e.g., superconductivity, metal-like conductivity, and metal–insulator transitions. One such group of compounds comprises reduced oxoniobates where niobium has an electron configuration between d^0 and d^1. So far, metal-like conductivity has only been found for Sr_xNbO_3 ($0.70 \leq x \leq 0.95$) and $Ba_{0.95}NbO_3$, both having the ideal perovskite-type structure (1–3). $CaNbO_3$ was first prepared by Lamure and Colas (4). Hervieu *et al.* later proposed that $CaNbO_3$ crystallizes with a distorted perovskite structure of $GdFeO_3$ type, space group *Pnma*, $a \approx c \approx \sqrt{2} \times a_{per}$, $b \approx 2 \times a_{per}$ (per = ideal perovskite) (5). However, neither structure nor resistivity data have been reported for $CaNbO_3$. Isawa *et al.* investigated the existence of a $Ca_{0.9-x}Sr_xNbO_3$ solid solution. They only obtained single-phase cubic perovskite-type samples in a narrow range, $0.7 \leq x \leq 0.9$, all exhibiting metal-like conductivity (6). The aim of the present study was to synthesize and characterize the whole range, $0 \leq x \leq 1$, of the $Ca_{1-x}Sr_xNbO_3$ solid solution.

EXPERIMENTAL

$Ca_{1-x}Sr_xNbO_3$ ($0 \leq x \leq 1$) samples were prepared by annealing pellets of appropriate mixtures of $Sr_5Nb_4O_{15}$, $5CaO \times 2Nb_2O_5$, and Nb (99.99%) in sealed, argon-filled niobium tubes at 1500°C for 6–20 h in a graphite furnace. After heating, the furnace was cooled to room temperature at a rate of 40–50°C/min. The precursors $Sr_5Nb_4O_{15}$ and $5CaO \times 2Nb_2O_5$ were prepared by heating stoichiometric amounts of MCO_3 (M = Ca, Sr) (99.99%) and Nb_2O_5 (99.99%) in air at 1200–1250°C for 24–48 h.

X-ray powder diffraction (XRD) patterns of all specimens were recorded with an FR-552 focusing camera, using Cu$K\alpha_1$ radiation ($\lambda = 1.54056$ Å) with germanium as an internal standard ($a = 5.6574$ Å). XRD data for the crystal structure refinement were collected on a STOE STADI-P powder diffractometer with a rotating sample in symmetric transmission mode. The monochromator was a germanium crystal, yielding $\lambda = 1.5406$ Å. The RIETAN-97 program package was used for the refinements (7).

Microanalyses of bulk samples were performed with a JEOL JSM 820 scanning electron microscope (SEM) with a LINK AN10000 energy-dispersive X-ray microanalysis (EDS) system. The cation content was calculated by averaging data from spot analyses of 8–12 crystallites. Electron diffraction (ED) studies and microanalyses of individual grains were made with a JEOL JEM 2000FX transmission electron microscope (TEM) operated at 200 kV. The microscope was equipped with a LINK QX200 energy-dispersive detector in high-angle position (70°). $Sr_5Nb_4O_{15}$ was used as an external standard for the EDS analysis in the TEM. The high-resolution electron microscopy (HREM) studies

[1] To whom correspondence should be addressed.

0022-4596/98 $25.00

were conducted with a JEOL JEM 3010 (1.7-Å point resolution) operated at 300 kV. For the TEM studies, small amounts of the sample were crushed in *n*-butanol. A drop of this dispersion was put on a holey carbon film supported by a copper grid.

The temperature dependence of the resistivity was measured between 1.5 and 300 K in a ^{4}He cryostat. Electrical contacts were prepared with silver paint, and this assembly was heat treated for 30 min at 300°C in flowing Ar gas to minimize the contact resistance. A conventional four-probe method was used. The resistance was measured using commercial multimeters (Solartron Schlumberger SB-7081 and Hewlett-Packard HP-3458) with full thermal compensation. The maximum resolution was 10 μΩ, and the typical sample resistance was about 10 mΩ. The temperature was monitored with a Pt thermometer from 20 to 300 K and with a graphite thermometer below 30 K.

RESULTS AND DISCUSSION

Synthesis

Monophasic samples of perovskite-type $Ca_{1-x}Sr_xNbO_3$ ($0 \le x \le 1.0$) compounds were obtained at 1500°C with 20-h annealing time. The color varied continuously from dark blue for $CaNbO_3$ to red for $SrNbO_3$. The compositions of these samples, as determined by EDS analysis in an SEM, are given in Table 1. These results show no indication of calcium at the niobium positions.

We found the annealing time to be an important parameter in the preparation of monophasic samples with high calcium content. For example, monophasic samples of stoichiometric $CaNbO_3$ were obtained by annealing for 20 h at 1500°C, whereas multiphase samples had formed after 8 h. In the latter case, EDS analysis revealed the main phase to be calcium rich (Ca : Nb = 55.7(0.3) : 44.3(0.3), at.%) relative to the stoichiometric composition obtained in the 20-h heating, which had a Ca : Nb ratio of 50(1) : 50(1) (see below). This suggests that the formation of stoichiometric $CaNbO_3$ occurs via a defective perovskite phase where Nb is partially replaced by Ca. The need for high synthesizing temperatures was also found by Hervieu *et al.*, who used 1400–1500°C when preparing monophasic samples of $CaNbO_3$ (5). Isawa *et al.* used lower annealing temperatures (1050°C) and accordingly did not obtain monophasic samples of $Ca_{0.9-x}Sr_xNbO_3$ for $x < 0.7$, which fits well in this picture (6). Their result is in agreement with our attempts to prepare $Ca_{1-x}Sr_xNbO_3$ compounds with high calcium contents ($0 < x < 0.8$) using evacuated silica tubes at 1200–1250°C for 6–48 h, resulting in black polyphasic samples. The black color indicates an oxidation state of niobium less than +5. The corresponding XRD patterns showed that several of the phases formed were of perovskite type, related to $(Sr,Ca)(Ca,Nb)O_3$ with Nb^{5+} (8).

TABLE 1
EDS Analysis Data for the $Ca_{1-x}Sr_xNbO_3$ ($0 \le x \le 1.0$) (1500°C) Solid Solutions

Nominal composition Ca : Sr : Nb (at.%)	EDS analysis data Ca : Sr : Nb (at.%)
50 : 0 : 50	50(1) : 0 : 50(1)
45 : 5 : 50	43(1) : 5(1) : 52(1)
40 : 10 : 50	37.0(5) : 10.5(5) : 52.5(5)
35 : 15 : 50	32(1) : 15.0(5) : 53(1)
30 : 20 : 50	26(1) : 21.0(5) : 53.0(5)
25 : 25 : 50	27(1) : 23(1) : 50(1)
20 : 30 : 50	18(1) : 30.0(5) : 52(1)
15 : 35 : 50	14(1) : 34(1) : 52(1)
10 : 40 : 50	9(1) : 39(1) : 52(1)
5 : 45 : 50	4(1) : 43(1) : 53(1)
0 : 50 : 50	0 : 48(1) : 52(1)

$CaNbO_3$

The crystal structure of $CaNbO_3$ was refined using X-ray powder diffraction data. As already mentioned, it has a perovskite-related structure with $a \approx c \approx \sqrt{2} \times a_{per}$ and $b \approx 2 \times a_{per}$. This supercell of perovskite is denoted I. The systematic absences indicated the space group to be *Pnma*. Initial atomic coordinates were taken from the crystal structure of $GdFeO_3$ (9). Individual isotropic displacement parameters were used for the cations, and a common one was used for the oxygen atoms. Crystallographic data for $CaNbO_3$ and details of the refinement, final atomic coordinates, and displacement parameters are given in Table 2. Observed, calculated, and difference X-ray diffraction patterns for $CaNbO_3$ are shown in Fig. 1. A structure model

TABLE 2
Crystallographic Data for $CaNbO_3$

Space group		*Pnma*			
Unit cell parameters[a]					
a (Å)		5.6526(2)			
b (Å)		7.9140(2)			
c (Å)		5.5323(2)			
V (Å^3)		247.49(2)			
Z		4			
2θ range, step (°2θ)		$10.0° \le 2\theta \le 100.0°$, 0.02°			
Number of reflections		139			
R_I, R_p		0.030, 0.076			
Atom	Position	*x*/*a*	*y*/*b*	*z*/*c*	B_{iso} (Å^2)
Ca	4*c*	0.046(1)	0.25	0.009(2)	1.3(2)
Nb	4*a*	0	0	0.5	0.64(5)
O1	4*c*	−0.026(4)	0.25	0.582(4)	0.1(3)
O2	8*d*	0.207(3)	−0.045(2)	0.801(2)	0.1(3)

[a] From Rietveld refinement.

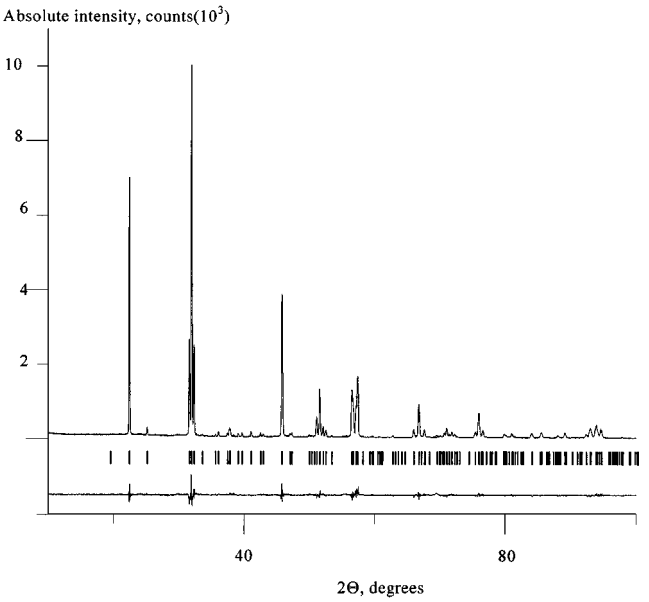

FIG. 1. Observed, calculated, and difference X-ray diffraction profiles for $CaNbO_3$.

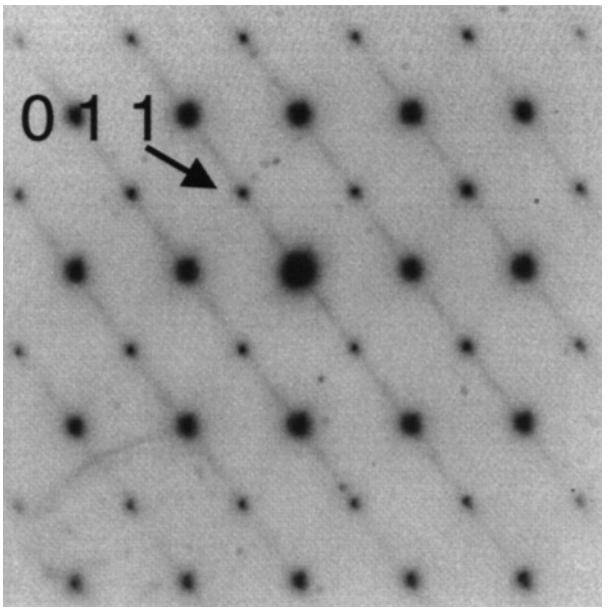

FIG. 2. $0kl$ electron diffraction pattern of $CaNbO_3$ with streaking along $\langle 111\rangle_{per}$. A $(011)_P = \frac{1}{2}\{111\}_{per}$ reflection is indexed.

with partial substitution of calcium for niobium was also tried. The initial occupancy of the 4*a* (Nb) position was changed to be 0.95Nb + 0.05Ca, and the corresponding thermal parameter was fixed at 1 $Å^2$ during the refinement. The obtained result indicated that only niobium atoms occupy the 4*a* position, in good agreement with the EDS analysis data (Table 1). Selected interatomic distances for $CaNbO_3$ are given in Table 3. The calcium atoms are surrounded by eight oxygen atoms, forming a bicapped trigonal antiprism with $d_{Ca-O} = 2.40(3)$–$2.76(2)$ Å. The Nb–O distances within the NbO_6 octahedra are 2.02(2)–2.07(2) Å, and the Nb–O–Nb angles between linked octahedra are 153(1)°. The Nb–O distances in $CaNbO_3$ are typical for Nb^{4+}–O. For example, in $Ba_{0.95}NbO_3$ (1) and in the room-temperature modification of NbO_2 (10), average Nb–O distances of 2.043 and 2.057 Å are found, respectively.

The ED patterns of $CaNbO_3$ were in agreement with the space group *Pnma* ($0kl$: $k + l = 2n$, $hk0$: $h = 2n$). However, kinematically forbidden $0k0$ reflections were occasionally found in the patterns, due to dynamical scattering. In the $\langle 110\rangle_{per}$ (per = ideal perovskite) diffraction patterns, streaking was often observed along $\langle 111\rangle_{per}$, as in the $h00_{per} = 0kl_P$ ($P = Pnma$) pattern of $CaNbO_3$ in Fig. 2. A lattice image showing these defects is seen in Fig. 3. They may be caused by a disordered substitution of Ca at the Nb positions in the $\{111\}_{per}$ planes, combined with cation vacancies according to the formula $A_{1-x}A'_xB_{1-y}B'_yO_3$, ($A$ = Ca, A' = vacancies, B = Nb, and B' = Ca at the Nb position). However, the EDS analysis and the Rietveld

TABLE 3
Selected Interatomic Distances (Å) and Angles (Deg) in $CaNbO_3$

Ca–O1	2.40(3)
–O1′	2.47(2)
–O2	2.40(2) (×2)
–O2′	2.68(2) (×2)
–O2″	2.76(2) (×2)
Nb–O1	2.035(5) (×2)
–O2	2.07(2) (×2)
–O2′	2.02(2) (×2)
Nb–O–Nb	153(1)

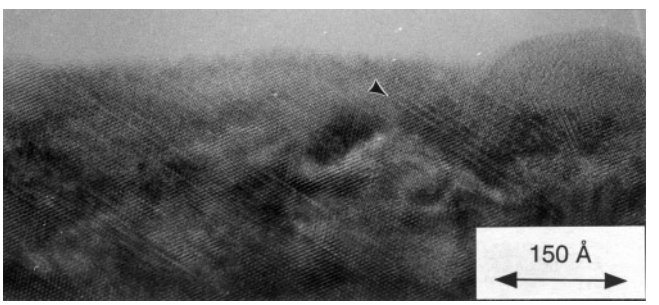

FIG. 3. HREM image corresponding to the ED pattern in Fig. 2 showing the defects (marked) causing the streaking in the ED pattern.

refinement discussed above show that the amount of calcium at the niobium position is small. The interpretation of the ED patterns and the HREM image is in agreement with the existence of the $Ca(Ca_xNb_{1-x})O_3$ ($0 \le x \le 0.33$) solid solution (5). In that system, the ED patterns for $x < 0.20$ exhibit superstructure reflections at $\frac{1}{4}\langle 111\rangle_{per}$, corresponding to a supercell with $a \approx 2 \times \sqrt{2} \times a_{per}$, $b \approx 4 \times a_{per}$, and $c \approx 2 \times \sqrt{2} \times a_{per}$ (denoted II) with space group *A2aa* or *Amaa*. (We have chosen an *A*-centered setting of the space group, instead of the *C*-centered setting given by Hervieu *et al.* to emphasize the relation to *Pnma* (5). They suggest that this supercell is caused by Ca atoms at the Nb positions.)

$SrNbO_3$

The perovskite Sr_xNbO_3 ($0.70 \le x \le 0.95$) is known to be cubic (1, 2, 11), but the XRD patterns of Sr_xNbO_3 ($x = 1.0$) samples annealed at 1550°C for 8 h in niobium ampoules reveal a distinct splitting of several strong reflections. The XRD patterns were indexed with a tetragonal unit cell having $a = 4.0242(1)$ and $c = 4.0320(1)$ Å. This result was supported by a closer inspection of the $(222)_{per}$ reflection, confirming it to be single, whereas the $(310)_{per}$ reflection was split. The unit cell volume is larger than for cubic $Sr_{0.95}NbO_3$ (1), indicating a higher Sr content. The SEM–EDS analysis showed the composition of this phase to be equal to that of stoichiometric $SrNbO_3$ within two esd's (see Table 1). This result was confirmed by TEM–EDS analysis, showing the average composition to be $Sr_{0.99(5)}NbO_3$. It should also be mentioned that Ridgley and Ward and Isawa *et al.* did not succeed in preparing monophasic samples of stoichiometric $SrNbO_3$ at 1000–1200°C using evacuated and sealed silica tubes (2, 11). Our findings suggest that the prepared $SrNbO_3$ has a strontium content higher than the upper homogeneity limit previously reported for Sr_xNbO_3 ($x = 0.95$).

The ED patterns of crystallites found in our $SrNbO_3$ sample exhibited weak superstructure reflections; ED patterns viewed along $\langle 100\rangle_{per}$ had superstructure reflections at $\frac{1}{2}\langle 110\rangle_{per}$. When the crystallites were tilted around $\langle 100\rangle_{per}$ and $\langle 010\rangle_{per}$, reflections corresponding to a doubling of all the unit cell axes were observed, as in the $\langle 130\rangle_{per}$ pattern of Fig. 4. This finding, together with the XRD data, suggests a tetragonal unit cell, $a \approx 2 \times a_{per}$ and $c \approx 2 \times a_{per}$. However, the crystallites consisted of several domains of different orientation, although oriented along the same pseudocubic zone axis. It should be mentioned that these superstructure reflections in most cases were very weak. Rietveld refinement using neutron diffraction data has shown the compound to be in fact orthorhombic ($a \approx \sqrt{2} \times a_{per}$, $b \approx 2 \times a_{per}$, and $c \approx \sqrt{2} \times a_{per}$,) and isostructural with $CaNbO_3$, space group *Pnma*. (12). This supercell is denoted IV.

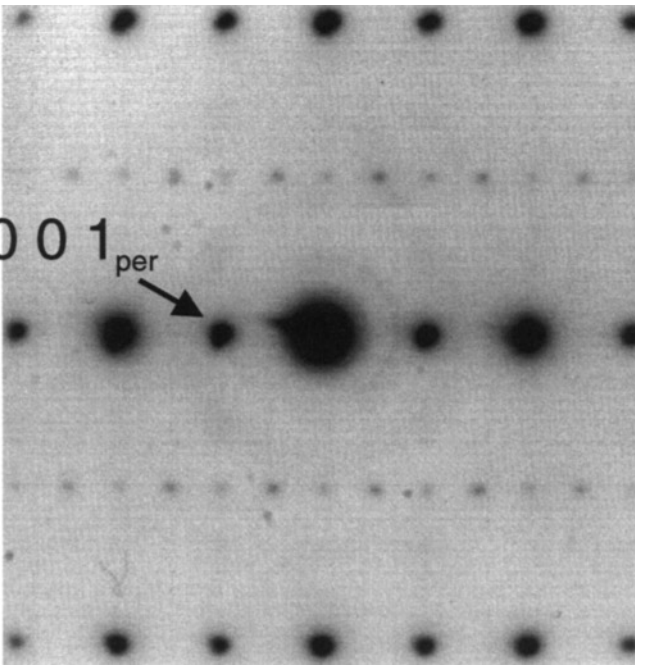

FIG. 4. ED along zone axis $\langle 130\rangle_{per}$ of $SrNbO_3$ (nominal composition, synthesized at 1550°C). The weak superstructure reflections are consistent with a type IV supercell ($a \approx \sqrt{2} \times a_{per}$, $b \approx 2 \times a_{per}$, and $c \approx \sqrt{2} \times a_{per}$).

$Ca_{1-x}Sr_xNbO_3$

The $CaNbO_3$ and $SrNbO_3$ compounds described above are the first and the last members of the $Ca_{1-x}Sr_xNbO_3$ ($0 \le x \le 1.0$) compositional series. The XRD patterns showed that all compounds formed in this series has perovskite-related structures. Their unit cell parameters as obtained from XRD data are given in Table 4. Only very weak

TABLE 4
Unit Cell Parameters (XRD) for $Ca_{1-x}Sr_xNbO_3$ ($0 \le x \le 1.0$) Solid Solution

x	Unit cell parameters (Å)
0	$a = 5.660(2)$, $b = 7.916(3)$, $c = 5.532(2)$
0.1	$a = 5.657(2)$, $b = 7.935(3)$, $c = 5.556(1)$
0.2	$a = 5.604(1)$, $c = 7.962(3)$
0.3	$a = 5.624(1)$, $c = 7.976(3)$
0.4	$a = 3.9913(4)$
0.5	$a = 3.9977(7)$
0.6	$a = 4.0064(5)$
0.7	$a = 4.0152(3)$
0.8	$a = 4.0277(3)$
0.9	$a = 4.0289(3)$
1.0	$a = 4.0242(1)$, $c = 4.0320(1)$

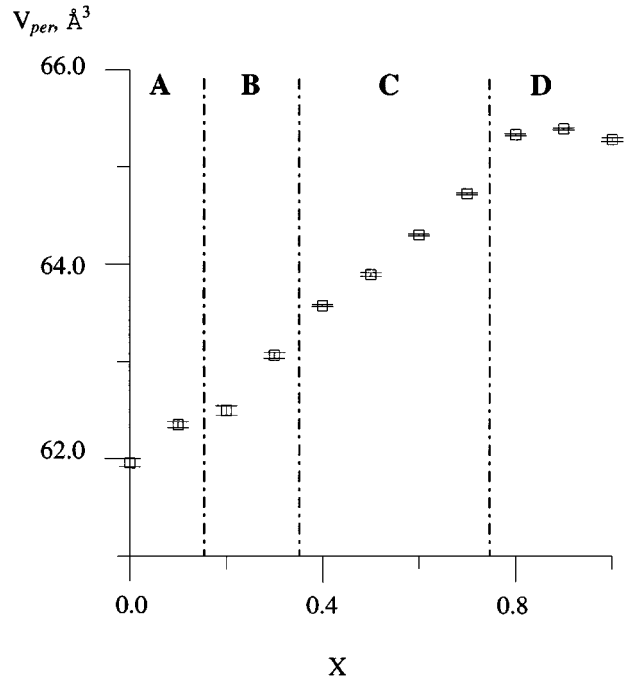

FIG. 5. Volume of the perovskite subcell (V_{per}) versus composition (x) for $Ca_{1-x}Sr_xNbO_3$. The figure is divided in to four regions based on the type of superstructures found by ED studies Region A: samples with crystallites exhibiting superstructure reflections corresponding to supercell I [$a \approx \sqrt{2} \times a_{per}$, $b \approx 2 \times a_{per}$, $c \approx \sqrt{2} \times a_{per}$ (the same as for $CaNbO_3$)], supercell II ($a \approx 2 \times \sqrt{2} \times a_{per}$, $b \approx 4 \times a_{per}$, $c \approx 2 \times \sqrt{2} \times a_{per}$), and an intergrowth between supercells I and II. Region B: Samples with crystallites exhibiting type II supercell ($a \approx 2 \times \sqrt{2} \times a_{per}$, $b \approx 4 \times a_{per}$, $c_A \approx 2 \times \sqrt{2} \times a_{per}$). Region C: Samples with crystallites exhibiting supercell III ($a_A \approx 4 \times a_{per}$). Region D: Samples with crystallites exhibiting a type IV supercell ($a \approx \sqrt{2} \times a_{per}$, $b \approx 2 \times a_{per}$, $c \approx \sqrt{2} \times a_{per}$).

reflections remained unindexed in the patterns. The corresponding perovskite subcell volumes versus composition are shown in Fig. 5. Electron diffraction studies were performed on selected samples ($x = 0.1$, 0.2, 0.5, 0.6, 0.8, and 0.9) in the series. All ED patterns observed had superstructure reflections relative to ideal perovskite. Four superstructure cells were identified:

$$\text{I, } a \approx \sqrt{2} \times a_{per}, \; b \approx 2 \times a_{per}, \text{ and } c \approx \sqrt{2} \times a_{per}$$

$$\text{II, } a \approx 2 \times \sqrt{2} \times a_{per}, \; b \approx 4 \times a_{per}, \text{ and } c \approx 2 \times \sqrt{2} \times a_{per}$$

$$\text{III, } a \approx 4 \times a_{per}$$

$$\text{IV, } a \approx \sqrt{2} \times a_{per}, \; b \approx 2 \times a_{per}, \text{ and } c \approx \sqrt{2} \times a_{per}.$$

I is the same supercell as discussed above in connection with $CaNbO_3$; supercell II is identical with that reported for $Ca(Ca_{1/3}Nb_{2/3})O_3$ (5), as mentioned above, and also for $Ca_{0.9}Sr_{0.1}(Ca_{1/3}Nb_{2/3})O_3$ (8). Supercell III has not been reported in the Ca–Sr–Nb–O system, whereas IV is similar to I and has also been found for $Ca_{0.45}Sr_{0.55}(Ca_{1/3}Nb_{2/3})O_3$ (8). On the basis of these findings, we have divided the $Ca_{1-x}Sr_xNbO_3$ compositional areas into four regions, marked A–D in Fig. 5.

Region A ($0 \le x \le 0.15$; *the compositional boundaries refer to Fig.* 5). Included in this region is $CaNbO_3$ with crystallites having defects. The ED study of the sample with $Ca_{1-x}Sr_xNbO_3$ ($x = 0.1$) showed the presence of three different types of crystallites: (i) The first crystallite type shows ED patterns of type I, corresponding to the same superstructure of perovskite as $CaNbO_3$. The systematic absences were in agreement with the space group *Pnma* for $CaNbO_3$. (ii) The second crystallite type has ED patterns with superstructure reflections indicating a type II supercell. Two ED patterns of this phase, taken along $\langle 110 \rangle_{per} = [100]_A$ and $\langle 111 \rangle_{per} = [012]_A$ ($A = A$ centered), are shown in Figs. 6a and 6b, respectively. In the $\langle 110 \rangle_{per}$ pattern there are strong superstructure reflections at $\frac{1}{4}\langle 111 \rangle_{per}$. On the basis of investigations of several crystallites, we conclude that the type II phase most probably ctystallizes in space group *Amaa* or *A2aa*. The interpretation is not straightforward, as most crystallites are twinned and consist of multiple domains of different orientation, although still oriented along the same pseudocubic zone axis, e.g., $\langle 110 \rangle_{per}$. The overlap of such domains can explain the weak reflections in the $[012]_A = \langle 111 \rangle_{per}$ pattern in Fig. 6b, which breaks the reflection conditions imposed from the *A*-centering. (iii) A third crystallite type was also frequently found. The corresponding ED pattern appeared to be an overlap between the type I and the type II patterns. An HREM image of such a crystallite viewed along $\langle 110 \rangle_{per}$ is shown in Fig. 7a. Alternating slabs of perovskite-related structures can be seen in the figure. The optical diffraction patterns of the slabs marked A and B are shown in Fig. 7b. The pattern of A is in agreement with a type II supercell viewed along $[100]_A = \langle 110 \rangle_{per}$, whereas that of B agrees with a type I supercell viewed along $[001]_P = \langle 110 \rangle_{per}$. These intergrowth crystallites thus seem to consist of alternating slabs of type I and II, with an intergrowth boundary approximately parallel to $\{110\}_{per}$, arrowed in Fig. 7. These slabs seem not to correspond to a variation in the Ca/Sr content as TEM–EDS analysis of crystallites without any intergrowth and having ED patterns in accordance with the superstructures I and II in this region showed the same cation ratio. The slabs are domains of I and II superstructures probably having the same chemical composition.

Region B ($0.15 \le x \le 0.35$). The XRD patterns of these samples were indexed tetragonally, with $a \approx \sqrt{2} \times a_{per}$ and $c \approx 2 \times a_{per}$. However, ED patterns of the $x = 0.2$ sample suggested a type II supercell. The ED patterns indicate the same space group, *Amaa* or *A2aa*, found for II in region *A*.

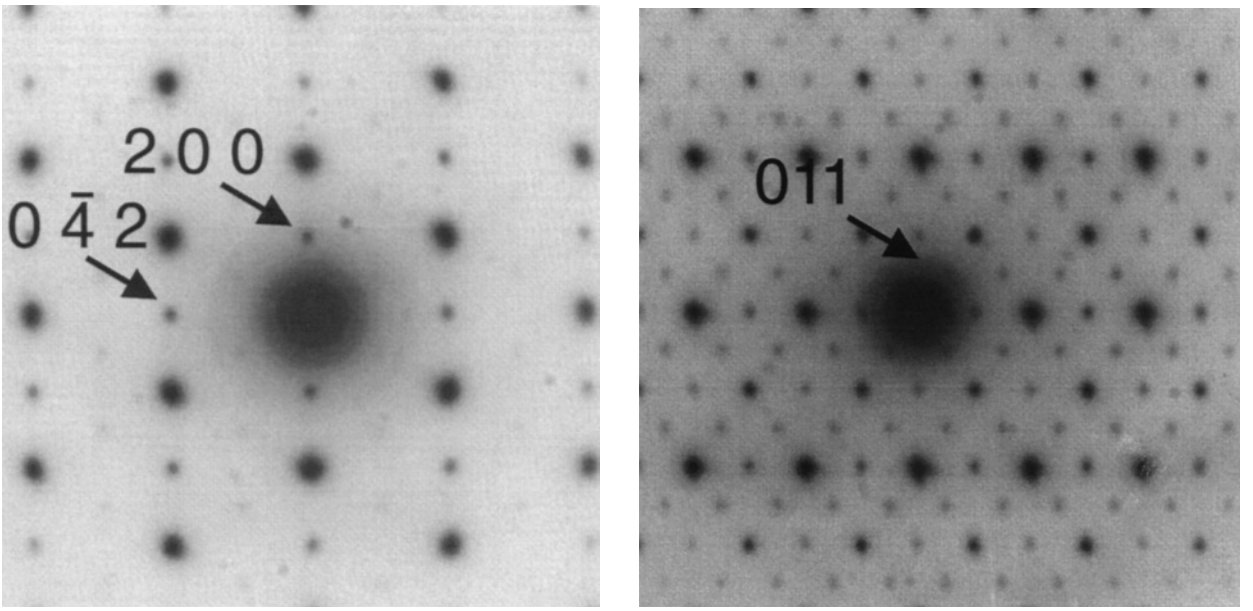

FIG. 6. Electron diffraction patterns of two crystallites with a type II supercell ($a_A \approx 2\times\sqrt{2}\times a_{per}$, $b_A \approx 4\times a_{per}$, $c_A = 2\times\sqrt{2}\times a_{per}$) found in a sample with nominal composition $Ca_{1-x}Sr_xNbO_3$ ($x = 0.1$). (a) A $[100]_A = \langle 110\rangle_{per}$ pattern ($A = A$ centered) with strong superstructure reflections at $\frac{1}{4}\langle 111\rangle_{per}$ consistent with space group *Amaa* or *A2aa*. (b) A $[012]_A = \langle 111\rangle_{per}$ pattern. The weak reflections (arrowed) must be caused by twinning, since they are inconsistent with an *A*-centered unit cell. The relations between the indexed supercell reflections and the perovskite subcell are (a) $(011)_A = \frac{1}{4}\{111\}_{per}$ and (b) $(04\bar{2})_A = \frac{1}{2}\{211\}_{per}$ and $(200)_A = \frac{1}{2}\{110\}_{per}$.

Region C ($0.35 \le x \le 0.75$). The XRD reflections of the $x = 0.4$ sample ($Ca_{0.6}Sr_{0.4}NbO_3$) showed no splitting up to 130° (2θ), indicating cubic symmetry. The monotonic dependence of reflection FWHM on 2θ diffraction angle fits into this model. TEM studies were performed on the $x = 0.5$ and 0.6 samples. All ED patterns obtained were consistent with an *F*-centered type III supercell with $a \approx 4\times a_{per}$. The ED patterns of two crystallites found in the $x = 0.6$ sample, taken along $\langle 001\rangle_{per} = [001]_F$ and $\langle 111\rangle_{per} = [111]_F$ (*F* stands for face centered), are shown in Fig. 8. Note that the $[111]_F$ pattern has a hexagonal intensity distribution, in contrast to the pattern in Fig. 6b, which is in agreement with cubic symmetry.

Region D ($0.75 \le x \le 1.0$). The XRD patterns of the $x = 0.8$ and 0.9 samples could be indexed with cubic unit cells, and that of $x = 1.0$ ($SrNbO_3$) with a tetragonal cell, as discussed above (see Table 4). In the $x = 0.9$ pattern, the reflections were clearly broadened, suggesting the true cell to be similar to that of $SrNbO_3$. The ED patterns of both $x = 0.8$ and 0.9 had superstructure reflections similar to those found in $SrNbO_3$, but their intensities were weaker. It is therefore very plausible that these compounds have the same supercell type IV as $SrNbO_3$ and that the orthorhombic distortion decreases with decreasing x in this region. However, the $x = 0.8$ sample can as well be ascribed to a cubic unit cell where $a = 2\times a_{per}$ and the $x = 0.9$ compound to a tetragonal unit cell ($a = b \approx 2\times a_{per}$ and $c \approx 2\times a_{per}$). (These supercells have been reported for $Sr(Ca,Nb)O_3$ (13)). To unambiguously determine which superstructure the $x = 0.8$ and 0.9 compounds have, a more detailed structural investigation using neutron diffraction data is needed. The small decrease in unit cell volume for the $x = 1.0$ compound relative to $x = 0.8$ and 0.9 can be explained by a very small change in the occupancy of the *A* site in ABO_3.

Resistivity Measurements

The resistivity of four samples was measured: $x = 0.0$, 0.1, 0.5, and 1.0. The normalized resistivity $R(T)/R(273)$ versus temperature is shown in Fig. 9. There is a transition from a metallic temperature dependence with positive $\partial\rho/\partial T$ at all temperatures for $x = 0.1$ and 1.0 to a nonmonotonic behavior for pure $CaNbO_3$, with $x = 0.0$. This sample also displays a marked upturn in the resistivity at low temperatures. For $x = 0.5$ (not shown) we observed approximately the same behavior as for $x = 0.1$ and 1.0.

The temperature behavior of the resistivity of $CaNbO_3$ can be explained by the fact that it is very similar to that observed, for instance, in the quasicrystal AlPdMn (14). In that case, the maximum in resistivity as a function of

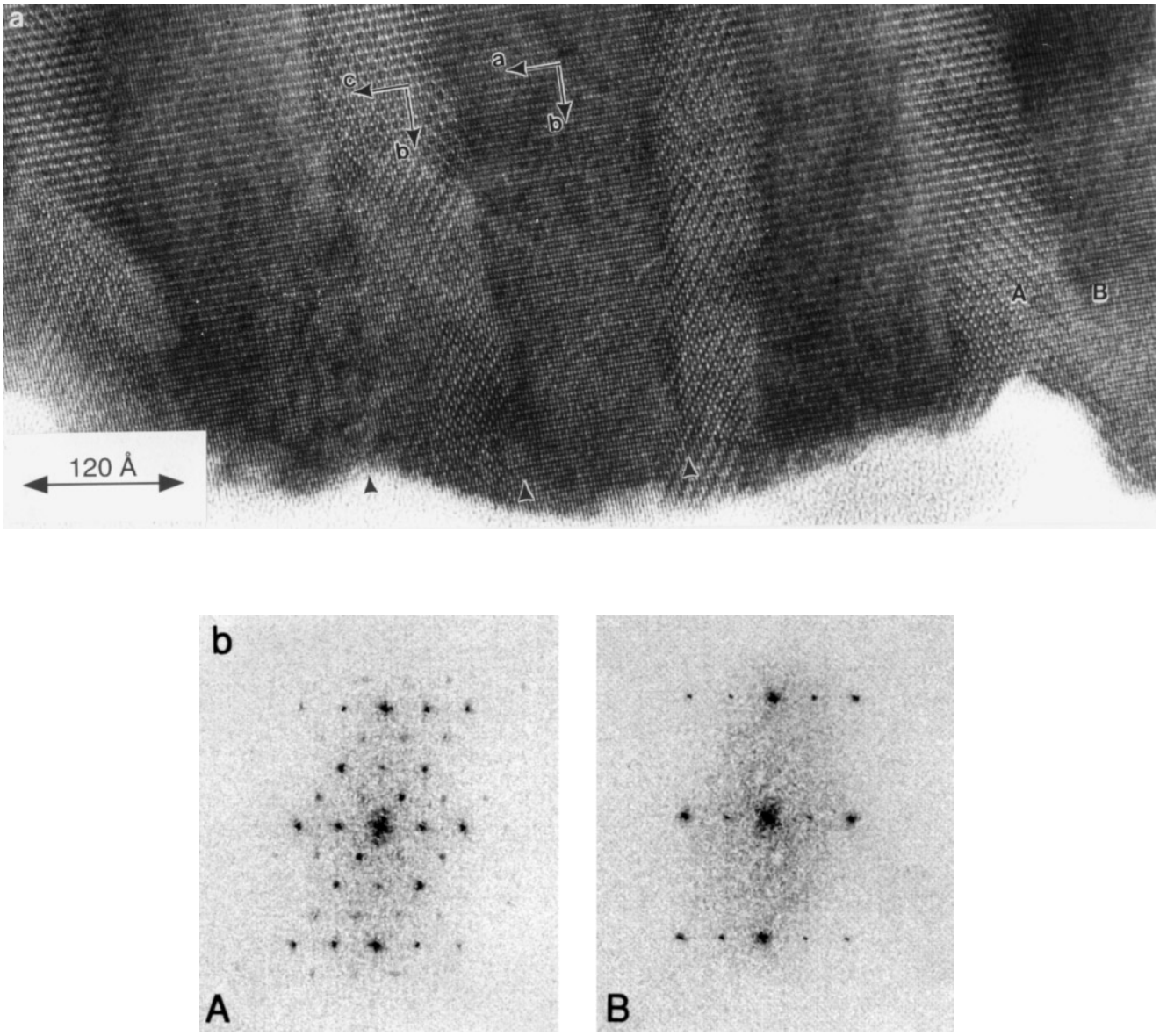

FIG. 7. (a) HREM image of a crystallite found in a $Ca_{1-x}Sr_xNbO_3$ ($x = 0.1$) sample, region B in Fig. 5. The crystal consists of alternating slabs of $CaNbO_3$ (one slab is marked B) and the type II supercell viewed along $[100]_A = \langle 110 \rangle_{per}$ ($A = A$-centered unit cell) (one slab is marked A). (b) Optical diffraction pattern of the slab marked A, corresponding to the A-centered supercell oriented along $[100]_A = \langle 110 \rangle_{per}$. B corresponds to a $CaNbO_3$ slab oriented along zero axis $[100]_P = \langle 110 \rangle_{per}$ ($P = Pnma$).

temperature can be explained in terms of quantum interference effects. We have tested this idea for our results and found that weak localization (15) can describe the temperature dependence if we exclude the sharp increase at low temperatures. Weak localization should be observable if the inelastic scattering time is long compared to the elastic scattering time. It is possible that the defects observed in the HREM images of $CaNbO_3$ (see Fig. 3) act as scattering centers, giving a shorter elastic scattering time than in Sr-containing samples with ordered superstructures. As for the sharp increase at low temperatures, we note that this is also seen in AlPdMn for certain compositions. In that case, it has been attributed to magnetic scattering, i.e., a Kondo effect, which also could be the case here.

CONCLUSIONS

We have found that substitution of Sr for Ca occurs in the whole $Ca_{1-x}Sr_xNbO_3$ compositional range. Compounds with perovskite-type structures were obtained at

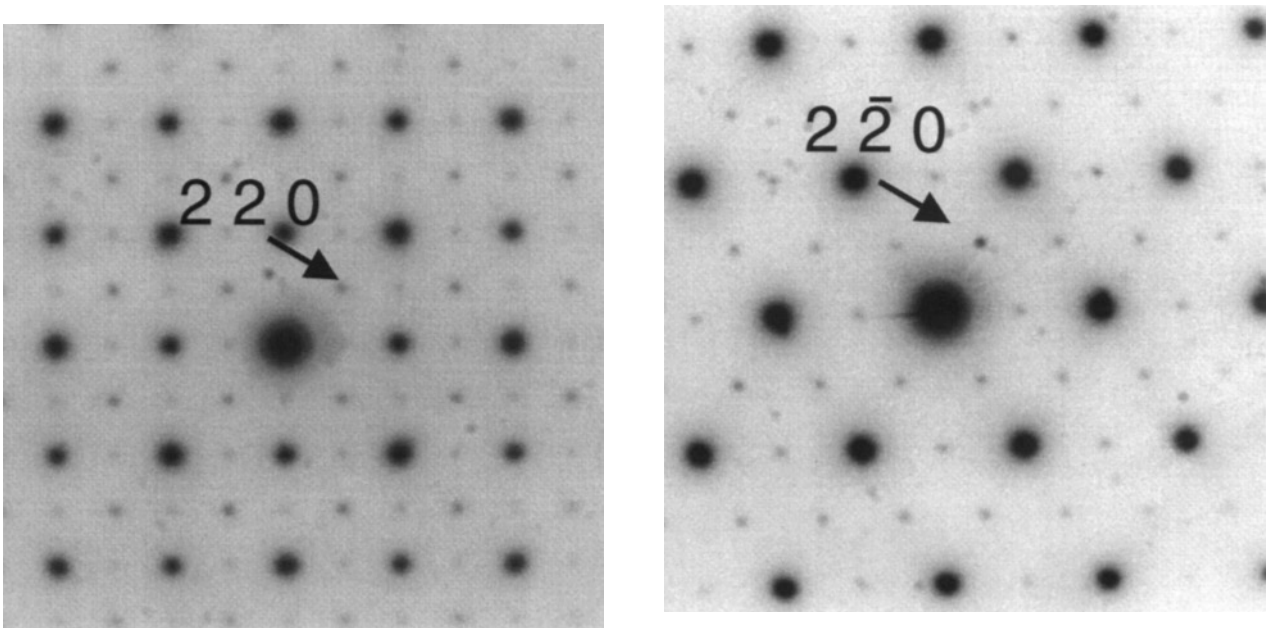

FIG. 8. ED patterns of two crystallites found in the sample $x = 0.6$, located in region C (see text), recorded along (a) $[001]_F = \langle 001 \rangle_{per}$ (F = face centered) and (b) $[111]_F = \langle 111 \rangle_{per}$. The ED patterns correspond to a type III supercell, i.e., an F-centered cubic unit cell with $a \approx 4 \times a_{per}$. The indexes refer to this unit cell, and the relationships to the perovskite subcell are (a) $(220)_F = \frac{1}{2}\{110\}_{per}$ and (b) $(02\bar{2})_F = \frac{1}{2}\{110\}_{per}$.

1500–1550°C for all compositions. The $GdFeO_3$-type crystal structure of $CaNbO_3$ has been refined. A new orthorhombic modification of Sr_xNbO_3 ($x = 1.0$) isostructural with $CaNbO_3$ has been synthesized. ED studies show that four different phase regions with various types of superstructures exist in the $Ca_{1-x}Sr_xNbO_3$ compositional range. Resistivity measurements showed $CaNbO_3$ to exhibit a nonmetallic behavior, whereas Sr-substituted samples were metal-like.

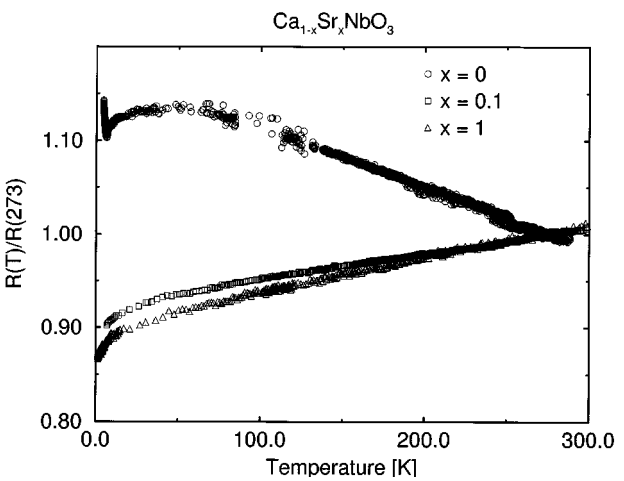

FIG. 9. Normalized resistivity ($R(T)/R(273)$) versus temperature for $Ca_{1-x}Sr_xNbO_3$ ($x = 0.0$, 0.1, and 1.0).

ACKNOWLEDGMENTS

W.H. thanks the Göran Gustafsson foundation for financial support and Dr. Östen Rapp for his kind interest. S.Ya.I. and O.G.D. thank Dr. E. M. Kopnin for valuable discussion and interesting ideas. This work has been supported by the Swedish Natural Science Research Council (NFR), the Royal Swedish Academy of Sciences, and the Russian Fundamental Research Foundation (Grant No. 97-03-33432a).

REFERENCES

1. B. Hessen, S. A. Sunshine, T. Siegrist, and R. Jimenez, *Mater. Res. Bull.* **26,** 85 (1991).
2. K. Isawa, J. Sugiyama, K. Matsuura, A. Nozaki, and H. Yamauchi, *Phys. Rev. B* **47,** 2849 (1993).
3. M. T. Casais, J. A. Alonso, I. Rasines, and M. A. Hidalgo, *Mater. Res. Bull.* **30,** 201 (1995).
4. J. Lamure and J.-L. Colas, *C. R. Acad. Sci. Paris* **270,** 700 (1970).
5. M. Hervieu, F. Studer, and B. Raveau, *J. Solid State Chem.* **22,** 273 (1977).
6. K. Isawa, R. Itti, J. Sugiyama, N. Koshizuka, and H. Yamauchi, *Phys. Rev. B* **48,** 7619 (1993).
7. F. Izumi, *Rikagu J.* **6,** 10 (1989).
8. M. Hervieu and B. Raveau, *J. Solid State Chem.* **28,** 209 (1979).
9. M. Marezio, J. P. Remeika, and P. D. Dernier, *Acta Crystallogr. Sect. B* **26,** 2008 (1970).
10. A. Bolzan, C. Fong, B. Kennedy, and C. Howard, *J. Solid State Chem.* **113,** 9 (1994).
11. D. Ridgley and R. J. Ward, *J. Am. Chem. Soc.* **77,** 6132 (1955).
12. H. Hannerz, S. Ya. Istomin, G. Svensson, and O. G. D'yachenko (to be published).
13. M. Hervieu and B. Raveau, *Rev. Miner.* **15,** 494 (1978).
14. H. Akiyama, T. Hashimoto, K. Shibuya, T. Edagawa, and S. Takeuchi, *J. Phys. Soc. Jpn.* **62,** 639 (1993).
15. H. Fukyama and K. J. Hoshino, *Phys. Soc. Jpn.* **50,** 2131 (1981).